BASIC STUDY

Acta Orthop Traumatol Turc 2013;47(5):359-365
doi:10.3944/AOTT.2013.2688

Characterization of powdered fish heads for bone graft biomaterial applications

Mustafa Özgür ÖTEYAKA[1], Hasan Hüseyin ÜNAL[2], Namık BİLİCİ[3], Eda TAŞÇI[4]

[1]*Department of Mechanical Engineering, Faculty of Engineering, Dumlupınar University, Kütahya, Turkey;*
[2]*Pendik Veterinary Control and Research Institute, İstanbul, Turkey;*
[3]*Directorate of Veterinary Affairs, Bahçelievler Municipality, İstanbul, Turkey;*
[4]*Department of Ceramic Engineering, Faculty of Engineering, Dumlupınar University, Kütahya, Turkey*

Objective: The aim of this study was to define the chemical composition, morphology and crystallography of powdered fish heads of the species *Argyrosomus regius* for bone graft biomaterial applications.

Methods: Two sizes of powder were prepared by different grinding methods; Powder A (coarse, d_{50}=68.5 µm) and Powder B (fine, d_{50}=19.1 µm). Samples were analyzed using X-ray diffraction (XRD), X-ray fluorescence (XRF), scanning electron microscopy (SEM), thermogravimetry (TG), and energy dispersive X-ray spectroscopy (EDS).

Results: The powder was mainly composed of aragonite ($CaCO_3$) and calcite ($CaCO_3$). The XRD pattern of Powder A and B matched standard aragonite and calcite patterns. In addition, the calcium oxide (CaO) phase was found after the calcination of Powder A. Thermogravimetry analysis confirmed total mass losses of 43.6% and 47.3% in Powders A and B, respectively.

Conclusion: The microstructure of Powder A was mainly composed of different sizes and tubular shape, whereas Powder B showed agglomerated particles. The high quantity of CaO and other oxides resemble the chemical composition of bone. In general, the powder can be considered as bone graft after transformation to hydroxyapatite phase.

Key words: Biomaterials; bone graft; calcium carbonate; characterization.

Natural biomaterials from the sea are promising alternatives for bone and dental implantation due to their availability (low cost) and ability to form the basis of bioceramics, especially the chemical compound $CaCO_3$.[1,2] Calcium carbonate, $CaCO_3$, is considered an inorganic precursor for inducing the formation of bioceramics.[3,4] Bioceramics such as hydroxyapatite $Ca_{10}(PO_4)_6(OH)_2$, tricalcium phosphate (TCP) and coralline scaffolds are widely used because they behave similarly to the mineral constituents of bone.[5,6]

LeGeros et al. compared the properties of shark enamel (impure calcium fluorapatite, idealized as ~$Ca_{10}(PO_4)_6F_2$) to those of human enamel (consists of impure calcium OH apatite, idealized as ~$Ca_{10}(PO_4)_6(OH)_2$) and reported that the contribution of fluorine is more significant than that of carbonate when both are present simultaneously in the apatite.[7] Manoli and Dalas used a biomineralization mechanism to repair bone around the implant.[8] Ions such as Ca^{2+} and PO_4^{-3} and OH- sites of hydroxyapatite and the pres-

Correspondence: Mustafa Özgür Öteyaka, MD. Dumlupınar Üniversitesi, Mühendislik Fakültesi, Makine Mühendisliği Bölümü, Evliya Çelebi Yerleşkesi, Kütahya, Turkey.
Tel: +90 274 - 265 20 31 e-mail: mozgur.oteyaka@dpu.edu.tr

Submitted: June 6, 2011 **Accepted:** May 30, 2012

Available online at
www.aott.org.tr
doi:10.3944/AOTT.2013.2688
QR (Quick Response) Code:

ence of several trace elements play important roles in overall physiological functioning and in the osseointegration process. Recently, several species of sea origin, such as the cuttlefish *Sepia officinalis*, the Chinese freshwater pearl powder, the Pacific Kumamoto oyster *Crassostrea sikamea*, and the bivalve mollusk *Venus verrucosa* have been characterized for their potential bioceramic materials.[9] Among them, nacre, or mother-of-pearl, is one of the most intensively studied materials.[10,11]

The shells of these animals are composed of both calcite (90%) and aragonite (10%) phases. The $CaCO_3$ mineral system consists of the following three anhydrous polymorphs in order of stability; calcite, aragonite and vaterite, which have rhombohedral, orthorhombic and hexagonal structures, respectively. The thermodynamically stable polymorph under normal conditions is calcite. Aragonite is metastable but its phase transformation to calcite is sufficiently slow to form geological formations. It has been reported that in bulk $CaCO_3$, the vaterite to calcite phase transition occurs at a temperature of ~560°C.[12] Lemos produced hydroxyapatite nanopowders from pure aragonite nacreous material (the polymorphic phase of $CaCO_3$).[13] The other metastable polymorph vaterite precipitates act as precursors under conditions of high supersaturation and transform to the stable phase within hours to days. However, it is still unknown how this phase transformation takes place with both an internal rearrangement and a dissolution/precipitation mechanism discussed.[12,14,15] Morphological analyses have been abundantly investigated; for example, shells of a conch (*Muricopsis* species) and of a terrestrial snail (*Helix* species) exhibit a principally cross-lamellar structure whereas the microarchitecture of nacre (mother-of-pearl) has been illustrated as a 'brick-and-mortar' arrangement.[15,16]

For biomaterial applications, it is important to know the chemical composition, crystal shape and morphology of $CaCO_3$. The amorphous phase of $CaCO_3$ plays a critical role in the initiation of the biomineralization process compared to the crystalline phase of $CaCO_3$; the solubility of amorphous $CaCO_3$ is about ten times higher than that of crystalline $CaCO_3$.[17]

In the present study, we aimed to report the preparation and characterization of a new biomaterial powder made from the fish heads (FH) of species *Argyrosomus regius* collected from the Turkish seas.

Materials and Methods

The powdered FHs of the *Argyrosomus regius* species used in this study were obtained from the Pendik Veterinary Control and Research Institute in Istanbul, Turkey. Powder A was created by placing FH pieces into a hardened-steel universal grinding vessel (Desktop Swing Mill HK40), milled for 1 minute and collected in a plastic sample holder. Powder A was then heated to 1000°C with steps of 10°C/min and then maintained at this temperature for 1 hour to complete the calcination period in the Protherm PLF 120/5 electric furnace. The obtained calcinate powder was coded Powder C. In addition, loss of ignition (LOI) for Powder A was calculated by measuring the difference in weight of the powder before and after heating to 1000°C.

Powder A was dry-milled using a Planetary micro mill Pulverisette 7 premium line for different milling times. Powder A was placed in the bowl made of stainless-steel and ZrO_2 balls at 600 rpm for 30 min. The obtained milled powder was coded Powder B.

The chemical compositions of the powders were determined. For this purpose, 4 g of Powders A and C were weighed and mixed with 0.9 g binding material and then pressed in a PE-EL press to (Breitländer GmbH, Wesel, Germany) form round tablet samples for X-ray fluorescence (XRF) testing. The crystallinity of Powders A, B and C were determined using an X-ray diffractometer (XRD, MiniFlex; Rigaku Corp., Tokyo, Japan) using Cu K(α) radiation with a Ni filter between 10 and 70°. The scanning speed was 2°/min with steps of 0.01°. Identification of the phases was achieved by comparing the experimental XRD patterns to Joint Committee on Powder Diffraction Standards (JCPDS) using the cards 71-2396 and 4-777 for aragonite and calcite. The weight loss of the powders with time were determined using a Diamond TG/DTA (PerkinElmer Inc., Waltham, MA, USA) thermal analyzer under a static nitrogen atmosphere at the heating rate of 10°C/min in the temperature range of 20° to 1100°C using platinum crucibles. The microstructure of the powders was examined using JEOL JSM 5600LV scanning electron microscope (SEM) with magnifications of ×500 and ×1500. The average particle size distribution of Powders A and B was measured using Mastersizer 2000 (Malvern Instruments Ltd., Worcestershire, UK) particle size analyzer.

Results and Discussion

The chemical analyses of Powder A and Powder C are presented in Table 1. Powder A was mainly composed of CaO (61.27%). The remainder of powder A was composed of different oxides in small quantities, such as SiO_2 (0.41%), Al_2O_3 (0.26%), SO_3 (0.17%), K_2O (0.16%), P_2O_5 (0.04%), Fe_2O_3 (0.04%), and organic matter. Furthermore, less than 0.02% was dedicated to

Table 1. Chemical compositions (wt %) of Powders A and C.

	Elements and oxides								
	Al_2O_2	SiO_2	P_2O_5	SO_3	K_2O	CaO	Fe_2O_3	Trace	LOI
Powder A	0.26	0.41	0.04	0.17	0.16	61.27	0.04	*<0.02	44.3
Powder C	0.26	0.45	0.04	0.06	0.20	80.44	0.01	†<0.01	.....

* Na_2O, MgO, TiO_2, V_2O_5, Cr_2O_3, MnO, Co_3O_4, CuO, ZnO, Ga, SrO, NiO, Ge, As_2O_3, Se, Br, Rb_2O, Y, ZrO_2, Nb_2O_5, Mo, Ag, CdO, In, SnO_2, Sb, Te, I, Ce, Ba, La, Wo_3, Hg, PbO, Th, U, Bi, Tl. †Na_2O, MgO, TiO_2, V_2O_5, Co_3O_4, MnO, Cr_2O_2

trace elements and oxides. The chemical composition of the FHs was quite similar to that of oyster shells in that it was principally composed of CaO (54.31 wt%), SiO_2 (1.25 wt%), Al_2O_3 (0.64 wt%), Fe_2O_3 (0.11 wt%), MgO (0.01 wt%), K_2O (0.01 wt%), Na_2O (0.93 wt%), and TiO_2 (0.11 wt%).[2] However, there was a higher quantity of CaO and other elements that are not present in shell, such as P_2O_5 (Table 1). P_2O_5 and the other elements mentioned in Table 1 can be beneficial for bone restoration purposes; Ca^{2+}, PO_4^{3-} and several trace elements play an important role in the osseointegration process.[2]

The chemical composition of Powder A was altered after the calcination treatment at 1000°C, principally due to volatile organic matter (Table 1). The first striking observation is that Table 1 shows an evident increase in the quantities of CaO, K_2O and SiO_2. The progress in CaO from 80.44 to 61.27 wt% can be explained by the decomposition of $CaCO_3$ to CaO and CO_2, where CO_2 is volatile:

$$CaCO_3 \rightarrow CaO+CO_2$$

Nevertheless, a slight decrease in SO_3 and Fe_2O_3 was found. In addition, no variation in the quantities of Al_2O_3 and P_2O_5 were registered and some trace elements disappeared after calcination (Table 1). The calcination treatment clearly showed a transformation of the phase and the presence of volatile matter. For this purpose, a LOI test was performed on Powder A.

The LOI test is part of an elemental or oxide analysis of a mineral or powder. The volatile materials that are lost are usually made up of organic matter and decomposing materials such as hydrates and carbon dioxide from carbonates. The quantity of the volatile organic matter was calculated from the difference in powder weight before and after heating to 1000°C. The LOI1000 test results confirmed that volatile constituents made up ~44.3% of Powder A.

Energy dispersive X-ray spectroscopy (EDS) was performed on Powder A (Fig. 1). Three principal peaks were observed. The most intense peak was dedicated to calcium (Ca), followed by oxygen (O) and carbon (C) with quantitative concentrations of 58.4 wt%, 39.9 wt% and 1.5 wt%, respectively. These results were in agreement with the conclusion obtained by XRF, especially for calcium. The sources of the C and O elements were most likely from the chemical compound $CaCO_3$. Additionally, EDS analysis was carried out after calcination. The concentrations of Ca (66.9 wt%) and C (2.2 wt%) increased while O (30.4 wt%) slightly decreased. Here, it should be noted that, as explained above, the decomposition of $CaCO_3$ and organic matter play a critical role in altering the quan-

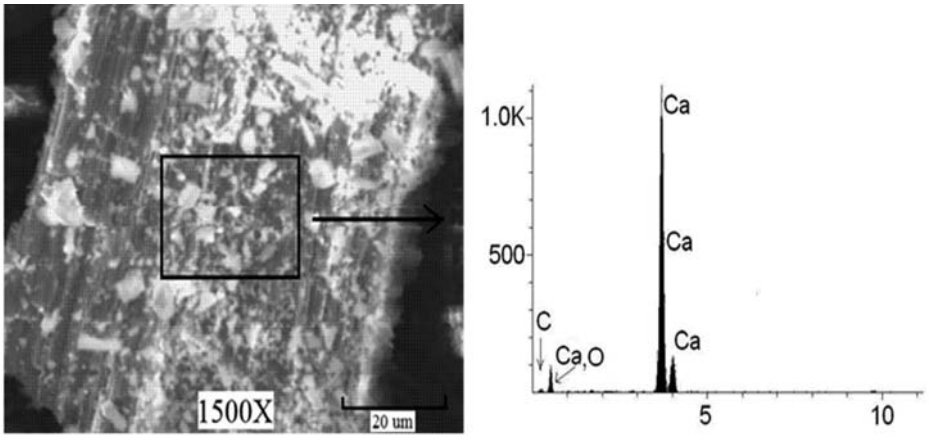

Fig. 1. EDS analysis of Powder A.

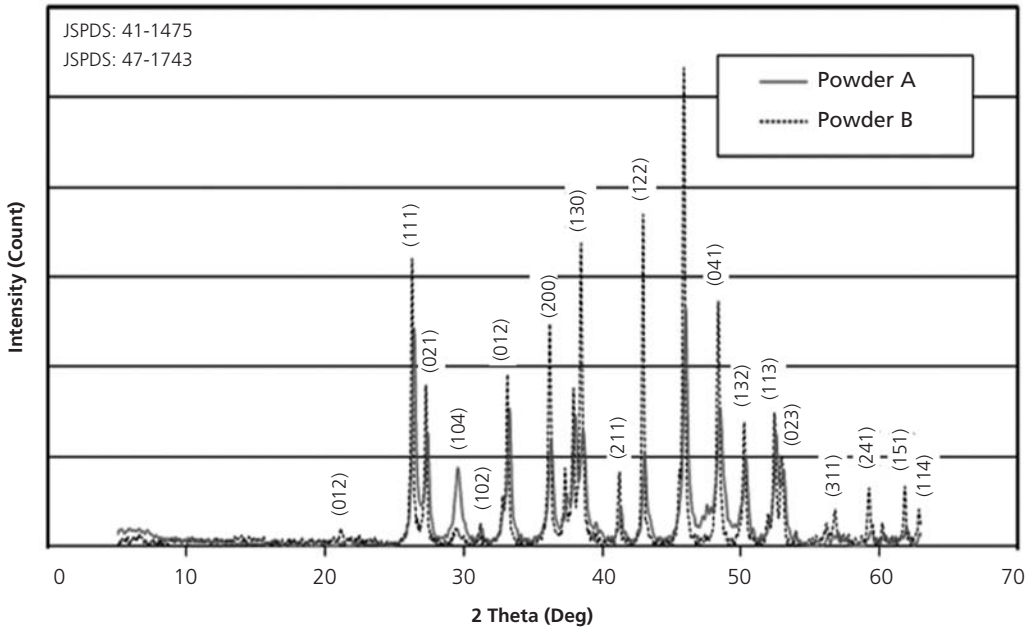

Fig. 2. XRD analyses of Powders A and B.

tity of elements, and increases in Ca and C are not surprising after calcination. The decrease in oxygen can be explained by the burning of volatile organic matter.

The chemical composition of the investigated powders included fundamental elements of bone, such as Ca, P and several trace elements as the inorganic composition of bone (bone mineral) is composed of carbonated hydroxyapatite $Ca_{10}(PO_4)_6OH_2$ with a lower crystallinity.

The XRD patterns of Powders A and B are presented in Fig. 2. At first glance, we can observe several peaks indicating the presence of a crystalline phase in

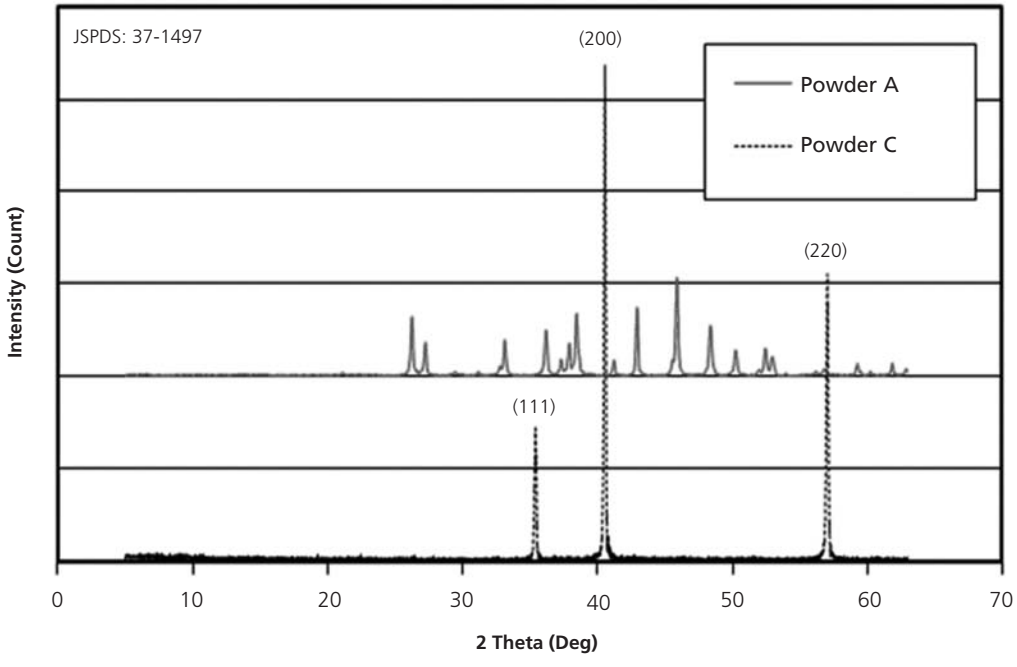

Fig. 3. XRD analyses of Powders A and C.

both materials. The diffractograms of Powders A and B match fairly well with the pattern of standard aragonite (JCPDS: 41-1475) and calcite (JCPDS: 47-1743). The vaterite phase, the third phase of $CaCO_3$, was not present as a peak. Therefore, the relative intensity of Powder B was more pronounced compared to the peaks of Powder A. For example, if we fit the peaks at 2Ø=29° for both materials, we can observe a huge difference in height and width. These differences can be attributed to the finer particle size distribution of Powder B.

In addition, we investigated calcinated powder in order to discover the phase transformation of Powder A. The XRD patterns of Powders A and C are presented in Fig. 3. The pattern of Powder C is composed of three intense peaks located at 2Ø=34.05, 2Ø=40.82 and 2Ø=56.74. As mentioned above, the diffractogram of Powder A matches fairly well with the patterns of the standard aragonite and calcite phases, while that of Powder C matches the standard calcium oxide (JCPDS: 37-1497). Here, we can conclude that calcination transforms the aragonite and calcite phases (Powder A) into the thermodynamically stable calcium oxide (Powder C).

The differential thermal analysis (DTA) and thermogravimetry (TG) of Powders A and B are plotted in Fig. 4. Both materials show a mass loss in two stages. The first stage, with a temperature range of 20° to 580°C, corresponds to the elimination of water molecules (removal of adsorbed water). Powders A and B had a weight loss of 1.8% (580°C) and 2.8% (570°C), respectively. The endothermic peaks of Powders A and Powder B were DTA_{max} = 246°C (-7.9 µV) and DTA_{max} = 369 °C (8.7 µV), respectively. The endothermic peak of the second stage, between 570° and 816°C, was related to the decomposition of $CaCO_3$ for both samples (DTA_{max} = 790°C for Powder A and DTA_{max} = 758°C for Powder B). However, it is difficult to predict which volatile and/or organic matter was removed. The quantity of lost materials was 41.8% (816°C) and 44.5% (778°C) for Powders A and B, respectively. The final solid product of the thermal decomposition was identified as calcium oxide, with a total mass loss of 43.6% and 47.3% for Powders A and B, respectively. These results are in agreement with the LOI test for the chemical composition analysis (Table 1). Here, we should note that an important difference in mass loss was observed between the two different sizes of powder; Powder B lost a mass 3.7% higher than Powder A. In addition, an area analysis of the endothermic peaks located at 790°C (637 µV s/mg) and 758°C (708 µV s/mg) for Powders A and B, respectively, concluded that there was a higher endothermic reaction for Powder B. This means that, at a low temperature, a greater decomposition of CaCO3 compared to CaO was realized with Powder B.

Fig. 5 and 6 show SEM images of Powders A and B at different magnifications. After grinding solid FH, the morphology of Powder A resembled a mixture of coarse bars (tubular) with different size particles (Fig. 5). The surface of the bars consisted of longitudinal lamellae,

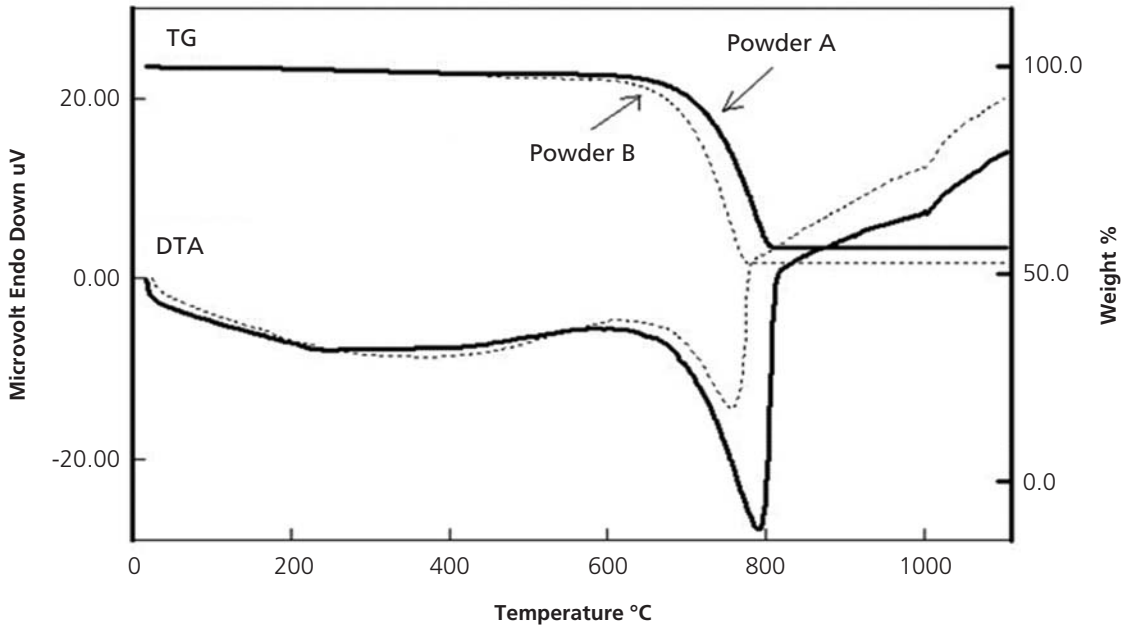

Fig. 4. DTA and TG of Powders A and B.

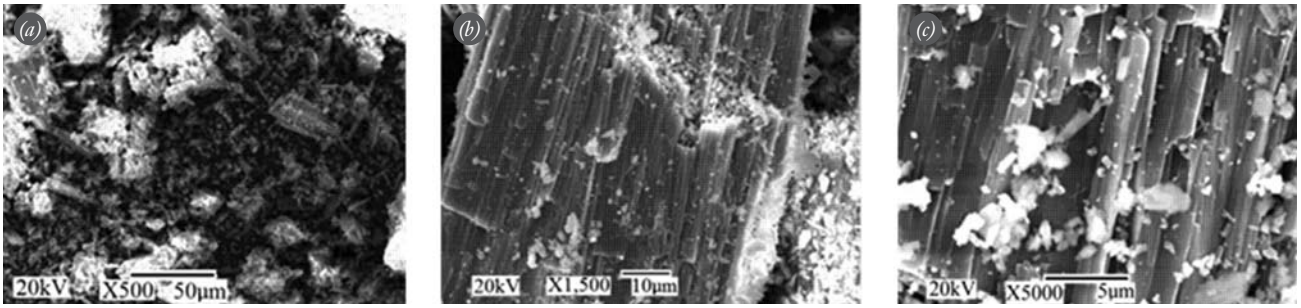

Fig. 5. **(a-c)** Scanning electron microscope images of Powder A at different magnifications.

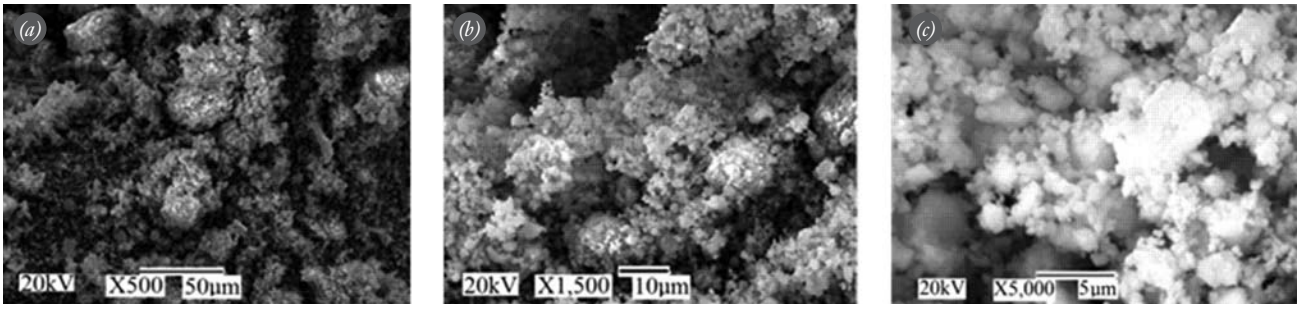

Fig. 6. **(a-c)** Scanning electron microscope images of Powder B at different magnifications.

probably formed during grinding (Fig. 5b), whereas the morphology of Powder B was composed of a network of small particles (Fig. 6). There was no doubt that the phenomenon of agglomeration was present in the structure of Powder B. It should be noted here that the coarse bars disappeared after ball milling.

The particle size distribution of Powders A and B are compared in Fig. 7. The particle size distribution of the products was determined as dry powders using the laser diffraction technique. It was found that the mechanical mixing Powder B had a smaller particle size than Powder A. Powder A had an average particle size distribution of d_{50} = 68.5 µm with d(0.1) = 2.1 µm and d(0.9) = 418.6 µm. Power B showed a smaller average particle size distribution of d_{50} = 19.0 µm with d(0.1) = 0.9 µm and d(0.9) = 96.90 µm. This result was in agreement with the SEM images presented in Figs. 5 and 6.

In conclusion, the chemical composition of powdered FH can be beneficial for bone graft preparations, especially the elements CaO, P_2O_5 and K_2O that are in

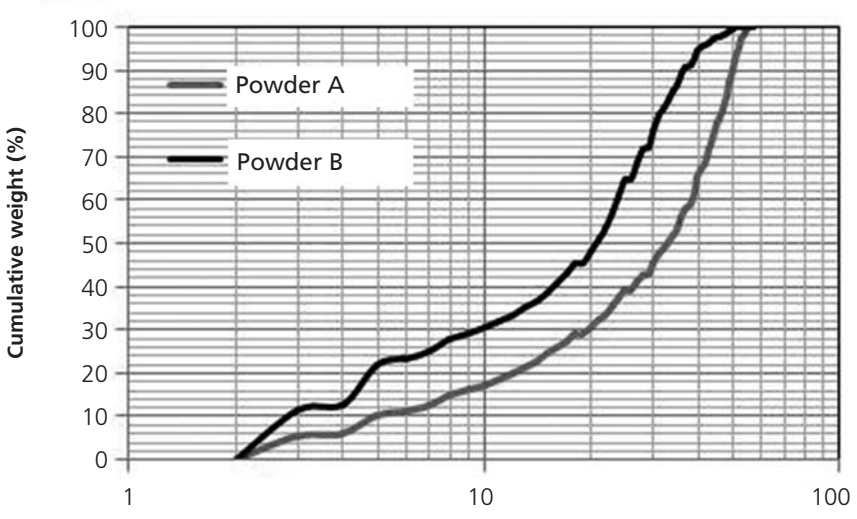

Fig. 7. Particle size distribution of Powder A and Powder B.

the composition of bone. The powder was principally composed of aragonite and calcite. Calcination at 1000°C transformed aragonite into the calcium oxide phase with a higher concentration of CaO. Planetary grinding decreased the size of Powder A from d_{50} = 68.5 µm to d_{50} = 19.0 µm (Powder B). However, agglomeration of the particles was observed in Powder B. For future work, Powder B should be transformed to hydroxyapatite with existing methods and should be compared with other bone grafts.

Acknowledgement

The author M. Ö. ÖTEYAKA expresses his gratitude to Pendik Veterinary Control and Research Institute for providing the fish heads and Dumlupınar University for technical support.

Conflicts of Interest: No conflicts declared.

References

1. LeGeros RZ. Calcium phosphate-based osteoinductive materials. Chem Rev 2008;108:4742-53.
2. Rocha JH, Lemos AF, Agathopoulos S, Valério P, Kannan S, Oktar FN, et al. Scaffolds for bone restoration from cuttlefish. Bone 2005;37:850-7.
3. Giannoudis PV, Dinopoulos H, Tsiridis E. Bone substitutes: an update. Injury 2005;36 Suppl 3:S20-7.
4. Ben-Nissan B. Natural bioceramics: from coral to bone and beyond. Curr Opin Solid State Mater Sci 2003;7:283-8.
5. Begley CT, Doherty MJ, Mollan RA, Wilson DJ. Comparative study of the osteoinductive properties of bioceramic, coral and processed bone graft substitutes. Biomaterials 1995;16:1181-5.
6. Dupoirieux L, Costes V, Jammet P, Souyris F. Experimental study on demineralized bone matrix (DBM) and coral as bone graft substitutes in maxillofacial surgery. Int J Oral Maxillofac Surg 1994;23:395-8.
7. LeGeros RZ, Silverstone LM, Daculsi G, Kerebel LM. *In vitro* caries-like lesion formation in F-containing tooth enamel. J Dent Res 1983;62:138-44.
8. Manoli F, Dalas E. Calcium carbonate crystallization on xiphoid of the cuttlefish. J Cryst Growth 2000;217:422-8.
9. Tüyel U, Öner ET, Özyegin S, Oktar FN. Production and characterization of bioceramic nanopowders of natural-biological origin. J Biotechnol 2007;131:S65-6.
10. Cartwright JH, Checa AG. The dynamics of nacre self-assembly. J Royal Soc Interface 2007;4:491-504.
11. Lopez E. Mother-of-pearl and the bone, the results show a promising alternative. Biofutur 2005;253:30-2.
12. Barriga C, Morales J, Tirado JL. Changes in crystallinity and thermal effects in ground vaterite. J Mater Sci 1985;20:941-6.
13. Lemos AF, Rocha JH, Quaresma SS, Kannana S, Oktar FN, Agathopoulos S, et al. Hydroxyapatite nanopowders produced hydrothermally from nacreous material. J Eur Ceram Soc 2006;26:3639-46.
14. Damien E, Revell PA. Coralline hydroxyapatite bone graft substitute: a review of experimental studies and biomedical applications. J Appl Biomater Biomech 2004;2:65-73.
15. Luz GM, Mano JF. Mineralized structures in nature: Examples and inspirations for the design of new composite materials and biomaterials. Compos Sci Technol 2010;70:1777-88.
16. Bertazzo S, Bertran CA. Morphological and dimensional characteristics of bone mineral crystals. Key Eng Mat 2006;309-311:3-6.
17. Becker A, Bismayer U, Epple M, Fabritius H, Hasse B, Shi J, et al. Structural characterisation of X-ray amorphous calcium carbonate (ACC) in sternal deposits of the crustacea *Porcellio scaber*. Dalton Trans 2003;4:551-5.